Table of contents:

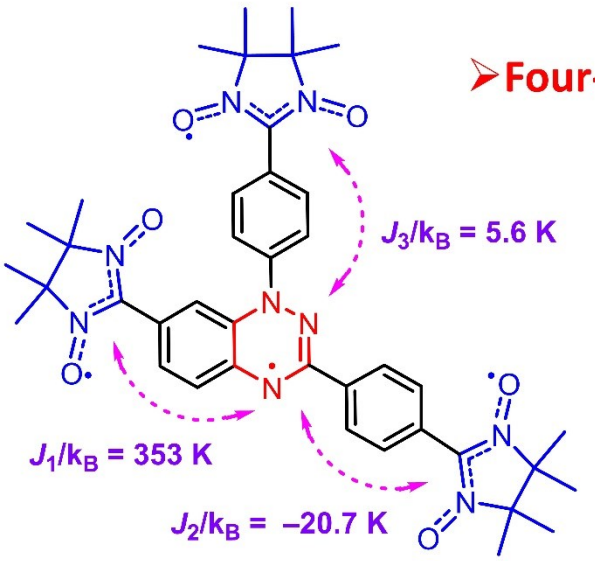

Tetraradical

➢ **Four-Spin Exchange-Coupled System**

➢ **Triplet Ground State and a Nearby Excited Quintet State**

➢ **High thermal stability**

➢ **Reversible redox waves**

Nitronyl Nitroxide-Substituted Benzotriazinyl Tetraradical

Evgeny V. Tretyakov,*[,1] Igor A. Zayakin,[1] Alexey A. Dmitriev,[2] Matvey V. Fedin,[3] Galina V. Romanenko,[3] Artem S. Bogomyakov,[3] Anna Ya. Akyeva,[1] Mikhail A. Syroeshkin,[1] Naoki Yoshioka,[4] Nina P. Gritsan*[,2]

[1] *N.D. Zelinsky Institute of Organic Chemistry, Russian Academy of Sciences, Leninsky Ave. 47, Moscow 119991, Russian Federation*
e-mail: tretyakov@ioc.ac.ru
[2] *V.V. Voevodsky Institute of Chemical Kinetics and Combustion, Siberian Branch of Russian Academy of Sciences, Institutskaya Str. 3, Novosibirsk 630090, Russian Federation*
e-mail: gritsan@kinetics.nsc.ru
[3] *International Tomography Center, Siberian Branch of Russian Academy of Sciences, Institutskaya Str. 3a, Novosibirsk 630090, Russian Federation*
e-mail: bus@tomo.nsc.ru
[4] *Department of Applied Chemistry, Faculty of Science and Technology, Keio University, 3-14-1 Hiyoshi, Kohoku-ku, Yokohama, Kanagawa 223-8522, Japan*
e-mail: yoshioka@applc.keio.ac.jp

ABSTRACT:

High-spin organic tetraradicals with significant intramolecular exchange interactions have high potential for advanced technological applications and basic research, but those synthesized to date possess limited stability and processability. In this work, we designed a tetraradical based on the Blatter's radical and nitronyl nitroxide radical moieties and successfully synthesized it using the palladium-catalyzed cross-coupling reaction of triiodotriazine with gold(I) nitronyl nitroxide-2-ide complex in the presence of a newly developed efficient catalytic system. The molecular and crystal structure of the tetraradical was confirmed by X-ray diffraction. The tetraradical possesses good thermal stability with decomposition onset at ~150 °C in an inert atmosphere. The tetraradical exhibits reversible redox waves (at −0.54 and 0.45 V vs Fc/Fc^+), unprecedented for high-spin tetraradicals. The magnetic properties of the tetraradical were characterized by SQUID magnetometry of polycrystalline powders and EPR spectroscopy in various matrices. The collected data, analyzed using high-level quantum chemical calculations, confirmed that the tetraradical has a triplet ground state and a nearby excited quintet state. The unique high stability of the prepared triazinyl-nitronylnitroxide tetraradical is a new milestone in the field of creating high-spin systems.

INTRODUCTION

Multispin organic systems, i.e., di-, tri-, and polyradicals, are intriguing molecules whose ground-state multiplicity can be manipulated by controlling intramolecular exchange interactions.[1–2,3,4] Among such multispin systems, molecules with high-spin ground states are of special interest due to their applicability to the design of fascinating functional materials.[5] For instance, such high-spin molecules have been proposed and investigated as building blocks for applications in organic batteries,[6,7] organic magnets,[8,9] spintronics,[10–11,12] spin filters,[13–14,15] memory devices,[16,17] and for the exploration of quantum interference with molecular conductivity.[18,19] However, their potential use for device fabrication depends not only on the intrinsic electronic properties, but also on stability and processability.[20] A number of kinetically stable radicals, including nitroxide, phenoxide, nitronyl nitroxide (NN), iminonitroxide, and oxoverdazyl radicals, have been known for many years.[21] Another exceptionally stable radical is the 1,2,4-benzotriazinyl radical synthesized by Blatter et al.[22] This type of radicals is currently gaining increasing importance due to the proposed efficient synthetic strategies,[23–24,25,26,27] which have paved the way to multifunctional paramagnetic agents with interesting magnetic properties.[28,29] Stable radical units have the distinct advantage that they can be attached to any organic moiety and can even be purified and crystallized under ambient conditions. When properly bridged (via ferromagnetic coupling units), all of these stable radicals have often been used as spin sources in the synthesis of high-spin ground-state organic molecules suitable for subsequent use as materials.[30–31,32] It is noteworthy that the simultaneous use of different types of radical units has proven to be particularly fruitful for the design of high-spin molecules, including those with a 1,2,4-benzotriazinyl core. Recently, Rajca *et al*. created the diradicals ^{t}Bu-Blt-NN and Blt-NN by appropriate coupling of the Blatter's radical with the nitronyl nitroxide radical via trimethylenemethane (TMM) topology.[33,34] The latter causes strong intramolecular ferromagnetic interactions between unpaired electrons. In addition, the diradicals ^{t}Bu-Blt-NN and Blt-NN have high thermal stability. Thus, according to thermogravimetric analysis, the diradicals ^{t}Bu-Blt-NN and Blt-NN begin decomposition at 175 and 160 °C, respectively. It should be noted that the Blt-NN diradical, the thermal occupancy of the triplet state of which is 95% at room temperature, can be evaporated in ultrahigh vacuum to form thin films on silicon. Then, Rajca *et al*. succeeded in synthesizing the triradical Blt-$(NN)_2$ with a quartet ground state, possessing two doublet−quartet energy gaps: $\Delta E_{DQ}^{1} \approx 0.2{-}0.3$ kcal·mol^{-1} and $\Delta E_{DQ}^{2} \approx 1.2{-}1.8$ kcal·mol^{-1}.[35] The Blt-$(NN)_2$ triradical has 70% occupancy of the quartet ground state at room temperature and good thermal stability with onset of decomposition at >160 °C in an inert atmosphere.

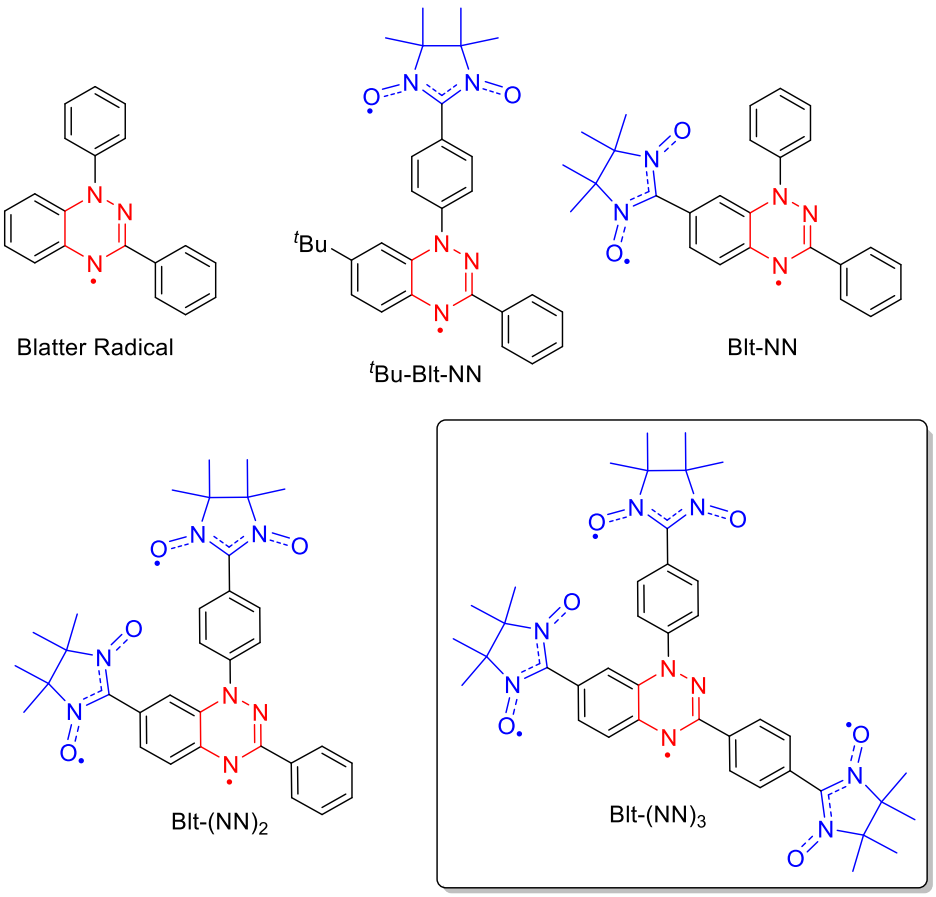

The next challenge is the high-spin tetraradical, possessing both good thermal stability under ambient conditions and a significant energy gap between the high-spin ground state and low-spin excited state. Tetraradicals with four unpaired electrons form a quintet as the ground state when all four spins are ferromagnetically coupled. If two unpaired electrons are coupled antiferromagnetically, then this situation leads to the formation of triplet ground state. Rajca *et al*. reported the synthesis of 1,3-linked poly(arylmethyl) quintet tetraradicals with a branched and cyclic structure by oxidation of the corresponding carbanions. Combined EPR/SQUID analysis revealed that all three tetraradicals possess a quintet ground state ($S = 2$); tetraradicals in the quintet state persist in the crystal state at ambient temperature for several days; in solution, decomposition is detected after a short period of time.[36] Recently, Rajca *et al*. succeeded in the synthesis of aminyl tetraradicals, also having a quintet ground state, as evidenced by SQUID magnetization and magnetic susceptibility measurements; the energy gap between the quintet and the nearest excited triplet state, $\Delta E_{TQ}/k_B$, is ≥150 K. Tetraradicals react with oxygen in solution at temperatures above 195 K and tend to form π-dimer-like structures in concentrated solutions.[37,38] Thus, up to date, neutral tetraradicals that are stable under ambient conditions and possess a significant energy gap between the high-spin ground state and low-spin excited state were unknown.

To solve the problem of the synthesis of high-spin tetraradicals, we turned to cross-coupling reactions involving organometallic derivatives of nitronyl nitroxide. The use of these reactions, discovered by Okada *et al.*,[39,40] opened up a completely new era for the creation of high-spin systems and for determination of their inherent magnetostructural correlations.[41] At the same time, the main limitation of this reaction, which prevents the realization of its full potential, is that it proceeds smoothly only with aryl iodides. In the case of di- and triiodoarenes, the cross-coupling reaction gives low yields of the target products. The reason is that the Okada's reagent (NN–Au–PPh_3), used in the first-generation catalytic system, has limited thermal stability and begins to decompose at temperatures of ~60–65 °C, at which cross-coupling reactions occur. Our systematic search[42,43] led to the creation of a second generation of organogold nitronyl nitroxide derivatives NN–Au–XPhos, NN–Au–^{Me}CgPPh and NN–Au–TTMPP, which have exceptionally high thermal stability and high reactivity in cross-coupling reactions even with diamagnetic aryl bromides.[44]

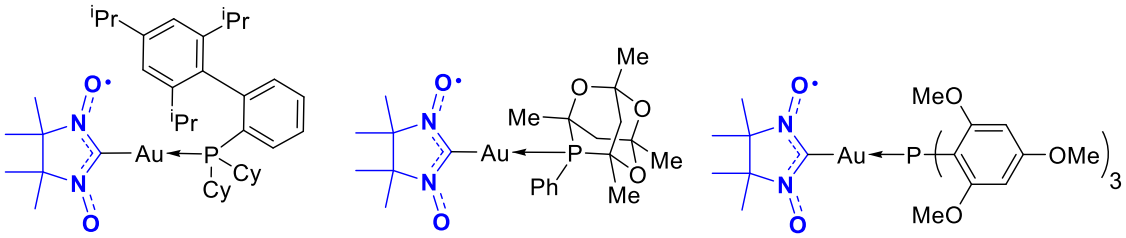

NN-Au-XPhos NN-Au-^{Me}CgPPh NN-Au-TTMPP

The Blatter moiety is significantly more electron-rich compared to typical diamagnetic π-systems. This is why cross-coupling reactions of the NN–Au–PPh_3 reagent with iodo derivatives of Blatter radicals were not efficient and resulted in low yields of the desired high-spin molecules.[35] Rajca investigated various reagents and catalytic systems and discovered that the cross-coupling of the Blatter diiodine radical with NN–Au–PPh_3 using a highly reactive Pd(0) catalyst (Pd[(*t*-Bu)$_3$P]$_2$) at a loading of 30 mol% allows the synthesis of the Blt-(NN)$_2$ triradical. Although the latter was obtained in acceptable isolated yields (19–42%), the applied catalytic system was not powerful enough for the triiodo-Blatter radical cross-coupling. In the present work, we propose an improved catalytic system that operates at room temperature and allows the preparation of cross-coupling products in high yields. Using this catalytic system, we successfully prepared and fully characterized the first tetraradical Blt-(NN)$_3$, which has both good thermal stability and a moderate energy gap between spin states of different multiplicity.

RESULTS AND DISCUSSION

Synthesis of Blt-(NN)$_3$. Cross-coupling of tri-iodo-Blatter radical (Blt-I$_3$) with 3.5 equiv. of NN–Au–PPh$_3$ with the help of the widely used Pd(PPh$_3$)$_4$ or the rarely applied Pd[(*t*-Bu)$_3$P]$_2$ (up to 30 mol%) forms a complex mixture of products with a small amount (<5%) of the isolated tetraradical Blt-(NN)$_3$. We also examined the recently proposed thermally stable reagent NN–Au–TTMPP[44] in the presence of Pd(PPh$_3$)$_4$. Using this reagent, the Blt-(NN)$_3$ tetraradical was obtained in acceptable yield (~60%). Careful selection of reaction conditions allowed us to find a simple and much more efficient method, which involves a cross-coupling reaction of Blt-I$_3$ with 3.5 equiv. of readily available NN–Au–PPh$_3$ in the presence of Pd$_2$(dba)$_3$ (40 mol%) and ^{Me}CgPPh (160 mol%) in toluene at room temperature. Remarkably, this methodology enabled the synthesis of the Blt-(NN)$_3$ tetraradical in a single step in high isolated yields (Scheme 1).

Scheme 1. Synthesis of tetraradical Blt-(NN)$_3$

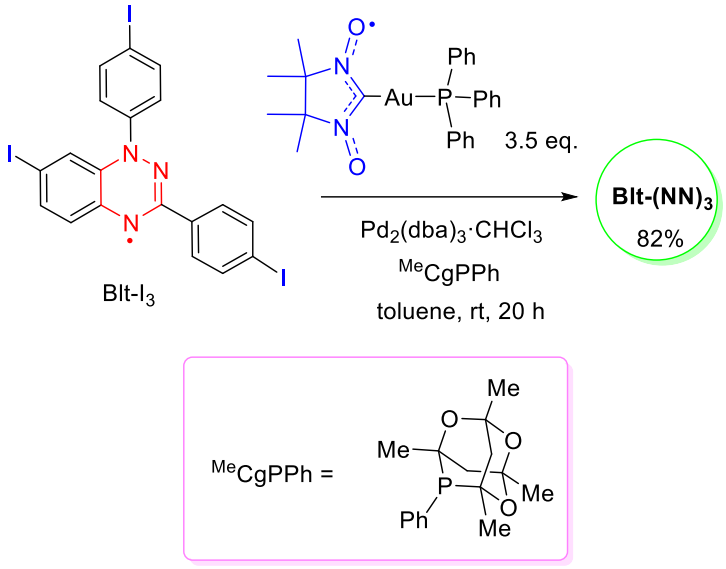

X-ray Crystallography. Single crystal X-ray diffraction analysis clarified the molecular structure and crystal packing in the solid state. Single crystals of the Blt-(NN)$_3$ tetraradical, suitable for X-ray diffraction analysis, were obtained by slow evaporation of solutions in CH_2Cl_2/heptane mixture at 5 °C. It was revealed that Blt-(NN)$_3$ crystallizes in the monoclinic space group $P2_1/c$ and contains one molecule of dichloromethane. Figure 1a shows the structure of the Blt-(NN)$_3$ molecule in ~~a~~ projection onto the plane of the 1,2,4-benzotriazinyl moiety. The N–O bond lengths in nitronyl nitroxide groups are in the range of 1.263(4)–1.284(5) Å; in the triazole ring, the lengths of all bonds are intermediate between double and single. Intramolecular O…O distances exceed 6 Å. The nitronyl nitroxide radical moieties A and B, as well as benzene ring B, are almost coplanar with the π-system of the 1,2,4-benzotriazinyl (Blatter) radical (Figure 2b). In the tetraradical, the torsion angles N(2A)C(11A)C(12A)C(13A), N(1)C(2)C(15B)C(14B)~~,~~ and

N(9B)C(11B)C(12B)C(13B) do not exceed 15° (Table 1). At the same time, the nitronyl nitroxide moiety C forms an angle of ~60° with the plane of the 1,2,4-benzotriazinyl moiety.

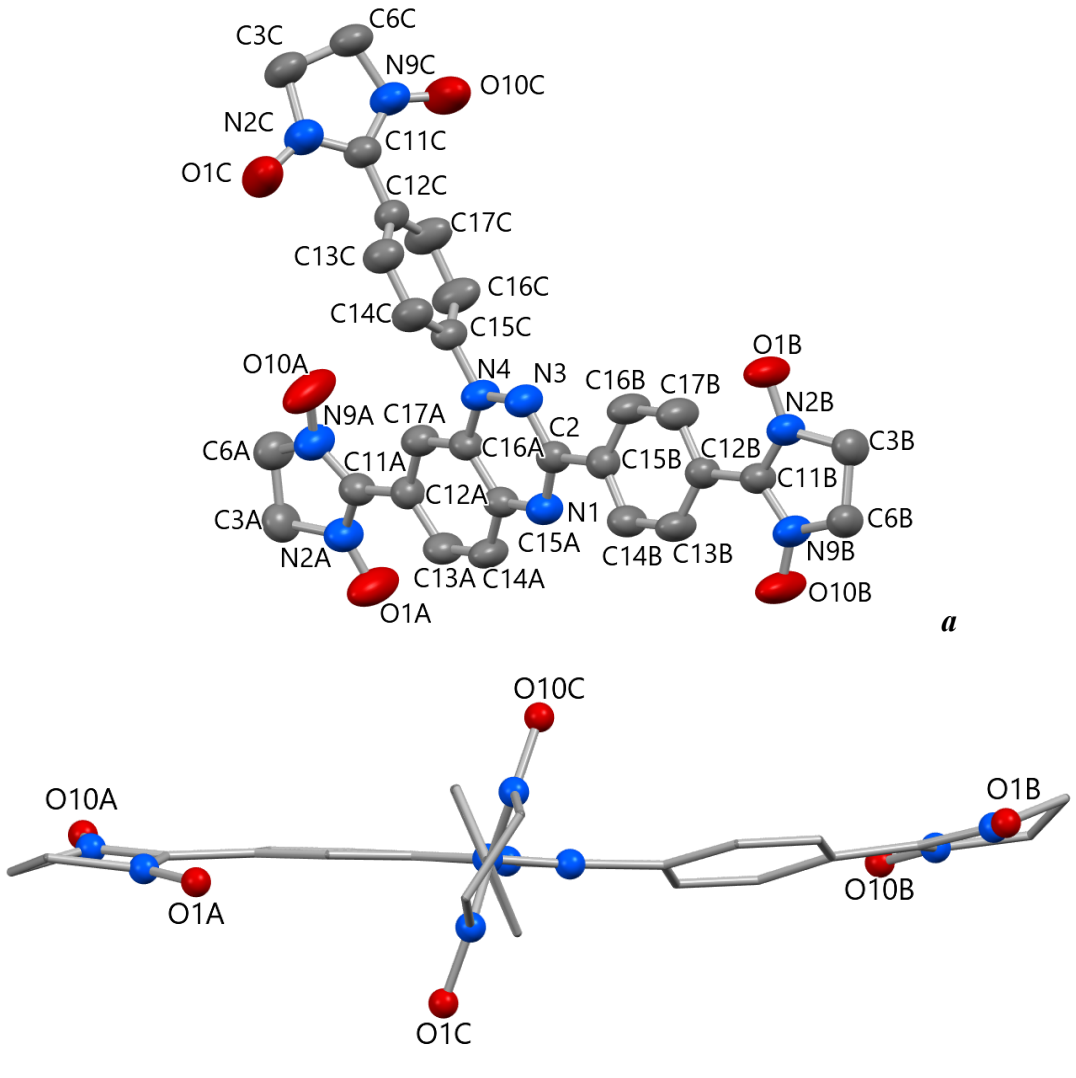

Figure 1. (*a* and *b*) Single-crystal X-ray structure of the Blt-$(NN)_3$ tetraradical in the projection on the Blatter moiety's plane, as well as the atom numbering scheme and a side view of Blt-$(NN)_3$. Parameters of atomic displacement are given with 50% probability; H atoms and CH_3 groups are omitted.

Table 1. Selected bond lengths, contacts (Å), and torsion angles (deg.) in Blt-$(NN)_3$.

Bond	d	Bond	d
O(1A)–N(2A)	1.263(4)	N(1)–C(15A)	1.356(4)
N(9A)–O(10A)	1.281(4)	N(1)–C(2)	1.347(4)
O(1B)–N(2B)	1.276(4)	C(2)–N(3)	1.336(4)
N(9B)–O(10B)	1.283(4)	N(3)–N(4)	1.363(4)
O(1C)–N(2C)	1.284(5)	N(4)–C(16A)	1.398(4)
N(9C)–O(10C)	1.278(5)	C(15A)–C(16A)	1.412(5)

		C(2)–C(15B)	1.482(5)
		N(4)–C(15C)	1.429(4)
Torsion angle	ω	Contacts	d
N(9B)C(11B)C(12B)C(13B)	6.4(3)	O(1A)…O(1B)[#]	3.698(5)
N(2A)C(11A)C(12A)C(13A)	–7.0(7)	O(1B)…N(1A)[#]	3.751(5)
N(1)C(2)C(15B)C(14B)	–15.0(6)	N(2B)…O(1A)[#]	3.522(5)
N(2C)C(11C)C(12C)C(13C)	–40.8(6)	N(4)…O(10C)[#]	3.630(5)
N(3)N(4)C(15C)C(14C)	–61.5(5)		
N(2B)C(11B)C(12B)C(13B)	–176.4(4)		

[#] –x, ½ – y, or –½ + z

The intermolecular distances between the paramagnetic centers, namely, the N, C and O atoms of the nitronyl nitroxide moieties and the N atoms of the Blatter π-system, exceed 3.5 Å (Figure 2b). The shortest of them, shown in Figure 2, are the intermolecular distances N(4)…O(10C') and O(1A)…N(2B'), equal to 3.630(5) and 3.522(5) Å, respectively. Moreover, O(1A)…N(2B') is the shortest distance between atoms of neighboring groups O(1A)-N(2A) and O(1B)-N(2B), located in parallel planes, but at an angle ~ 40° to each other.

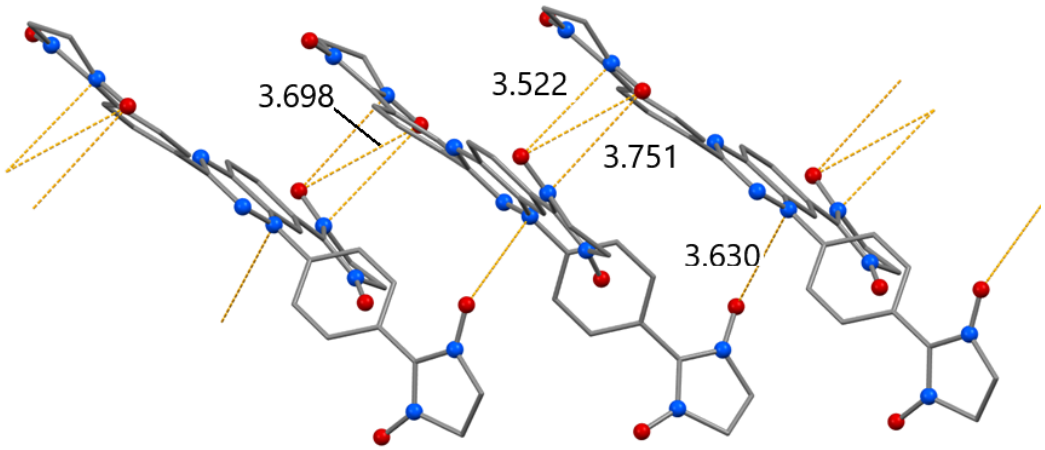

Figure 2. The shortest intermolecular distances N…O in Blt-$(NN)_3$.

EPR Spectroscopy. The continuous wave (CW) EPR spectrum of the Blt-$(NN)_3$ tetraradical in toluene solution at room temperature consists of a single line without a resolved structure (Fig. 3). For comparison, Figure 3 also presents the EPR spectrum of the oxoverdazyl-nitronyl nitroxide triradical, previously recorded under similar conditions.[4]

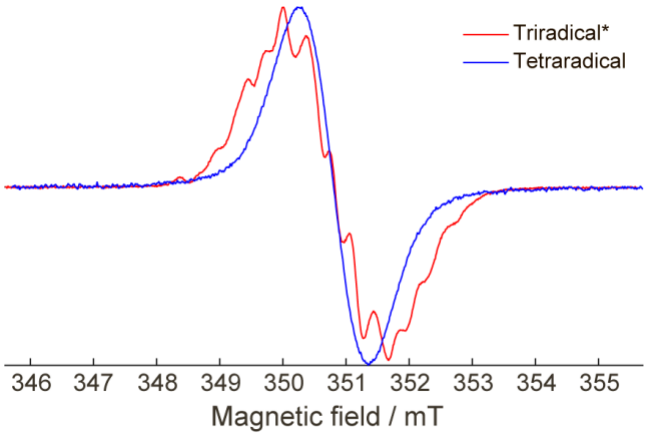

Figure 3. CW EPR spectra recorded at room temperature in toluene solution for Blt-$(NN)_3$ (blue) and the reference triradical.[4]

It is noteworthy that the EPR spectrum of the Blt-$(NN)_3$ tetraradical is narrower compared to that of the reference triradical, as would be expected for polyradicals composed of similar monoradical units. Indeed, the effective hyperfine interaction constants decrease in proportion to the number of electron spins due to exchange interaction, as illustrated, in particular, in our previous papers for the series monoradical – diradical – triradical.[3,4] Thus, the continuation of this trend for the Blt-$(NN)_3$ tetraradical in the present work does confirm the presence of four exchange-coupled electron spins in the molecule.

Pulsed EPR spectra of Blt-$(NN)_3$ were also recorded in toluene glass in the temperature range 6–80 K. Obtaining CW EPR spectra in this temperature range was problematic due to long electronic spin relaxation, leading to microwave saturation and distortion of the lineshape; however, EPR spectra detected by free-induction decay (FID) could be easily obtained (Figure 4).

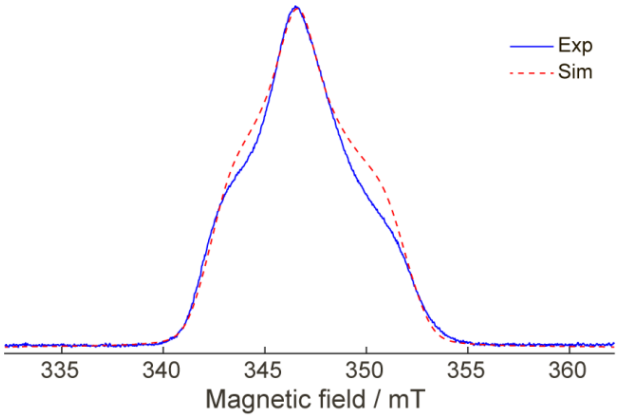

Figure 4. FID-detected EPR spectrum of Blt-$(NN)_3$ in toluene glass at 40 K (blue) and corresponding simulation in a model assuming the triplet state ($S = 1$) of the tetraradical (dashed red curve; see text for parameters).

There are no dramatic changes in the spectrum in the range T = 6–80 K (Figure S2, SI); only minor alterations in relative intensities were observed between the global maximum and the shoulders. Therefore, most likely, in this temperature we see the same spin state. The spectrum can be modeled by a triplet state (S = 1) with a zero-field splitting parameter D = 5 mT (E/D = 0.33) and an axial g-tensor ($g_{||}$ = 2.003, $g_{\perp}$ = 2.009). The slight discrepancy in side arm intensity with experiment is likely due to orientation-dependent transverse relaxation, which is also in line with similar spectral changes with temperature shown in Figure S2. The observed triplet state was assigned to the ground state of the Blt-$(NN)_3$ tetraradical in accordance with quantum chemical calculations. However, the nearby excited quintet state did not manifest itself in the FID-detected EPR, although this state should also be largely populated in the temperature range discussed. Most likely, the quintet state is invisible in FID-detected EPR spectra due to the much faster electron spin relaxation compared to the triplet state. Note that this shortening of spin relaxation time with the increasing number of electron spins is a well-known and generally anticipated trend.[45]

Thus, the combination of CW EPR in solution and pulsed EPR in the glassy-state made it possible to confirm the presence of four electron spins per molecule and to observe the ground triplet state of the Blt-$(NN)_3$ tetraradical.

SQUID Magnetometry and Quantum Chemical Analysis. The bulk magnetic properties of the Blt-$(NN)_3$ tetraradical were experimentally investigated by SQUID magnetometry of polycrystalline samples. At 300 K, χT was found to be 1.64 $cm^3 \cdot K \cdot mol^{-1}$, which is between the theoretical values of 1.5 $cm^3 \cdot K \cdot mol^{-1}$ for four noninteracting spins S = 1/2 and 1.75 $cm^3 \cdot K \cdot mol^{-1}$ for two noninteracting spins S = 1/2 and one paramagnetic center with spin S = 1. This indicates one fairly strong ferromagnetic exchange interaction and two much weaker interactions. With decreasing temperature, χT decreases monotonically reaching 1.50 $cm^3 \cdot K \cdot mol^{-1}$ at 70 K, and then declines more rapidly to 0.42 $cm^3 \cdot K \cdot mol^{-1}$ at 2 K (Figure 5). The latter value may indicate the close proximity of the triplet (χT =1.0) and singlet states of the Blt-$(NN)_3$ tetraradical, although intermolecular antiferromagnetic interactions can also affect the χT values at cryogenic temperatures. To shed light on the nature of the observed magnetic behavior of the Blt-$(NN)_3$ tetraradical, intra- and intermolecular exchange interactions were calculated by quantum chemical methods using the XRD crystal structure.

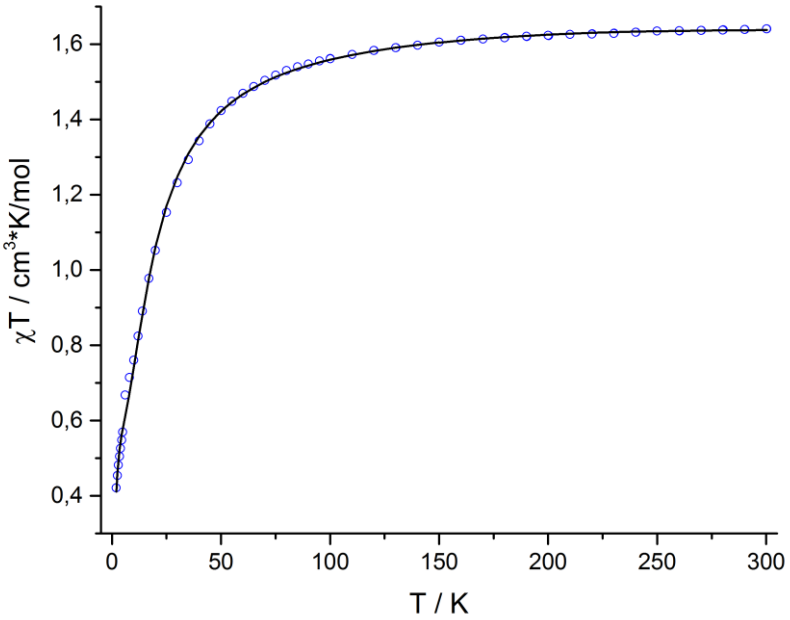

Figure 5. Experimental temperature dependence of χT (blue circles) for polycrystalline samples of tetraradical Blt-$(NN)_3$ in a field of 5 kOe. Black line corresponds to the best fit with four fitting parameters.

The Blt-$(NN)_3$ tetraradical has 6 low-lying spin multiplets (1 quintet, 3 triplet and 2 singlet states), resulting from exchange interactions of four radical centers. The energies of these multiplets were calculated at the SA-CASSCF(12,12)/NEVPT2/def2-TZVP level. Figure S3.1 (SI) represents the molecular orbitals (MOs) of the active space, four of which are almost degenerate (MO_{197} – MO_{200}) and localized on the NN and Blt radical moieties. According to calculations, the Blt-$(NN)_3$ tetraradical has a ground triplet state, with the first excited state predicted to be a quintet state, followed by a singlet state (Table 2, for details see Supporting Information, Section S3).

Table 2. Relative energies and multiplicities of low-energy spin states of the Blt-$(NN)_3$ tetraradical calculated at the CASSCF(12,12)/NEVPT2/ def2-TZVP level and estimated using the PHI program and J values calculated at the CASSCF(10,10)/NEVPT2/ def2-TZVP level, as well as using the best-fit J parameters.

2S + 1	CASSCF(12,12)/ NEVPT2 calculations	2S + 1	Evaluated using calculated J values		2S = 1	Evaluated using the best-fit $J_1 - J_3$
			$J_1 - J_3$	$J_1 - J_6$		
3	0	**3**	0	0	**3**	0
5	7.0	1	12.2	12.0	1	5.1
1	23.2	**5**	24.9	27.3	**5**	21.3
3	30.6	3	37.8	39.1	3	26.6
3	540.2	1	517.0	518.3	3	506.4
1	540.7	3	517.7	518.5	1	506.6

However, to better understand the nature of magnetic properties, we also calculated parameters of the pair exchange interactions ($\hat{H}_{ij} = -2J_{ij}\hat{\hat{S}}_i\hat{\hat{S}}_j$) for model diradicals obtained by adding hydrogen atoms to the remaining radical fragments (Figure 6 and Figure S3.3). The J parameters were calculated at the CASSCF and CASSCF/NEVPT2 levels, as well as using the spin-unrestricted broken-symmetry (BS) approach (for details see discussion in SI, Section S.3). Results of these calculations are presented in Table 3 and Table S3.2.

Table 3 shows that all types of calculations predict the same signs of the parameters J_i, however, calculations at the BS-DFT level give significantly overestimated absolute J values. It is also clear that the parameters of exchange interactions between NN fragments ($J_4 - J_6$) are very small and they can be neglected in the analysis of magnetic properties. In turn, the absolute values of $J_1 - J_3$ differ significantly, and J_1 is really large ($2J_1/k_B$ = 713 K), which explains why the χT value at 300 K noticeably exceeds the theoretical value for four non-interacting spins 1/2 (Figure 5). The large positive value of J_1 is explained by the McConnel I mechanism[46] (Figure S3.1, SI), since the radical fragments are connected by a C–C bond, in which the C atom of the NN fragment has a large negative spin population (–0.19), and the C atom of the Blatter radical fragment (Blt) has a large positive spin population (0.11). The difference in the sign of J_2 and J_3 could be explained by the difference in the mutual arrangement of the NN and Blt fragments (SI, Section 3).

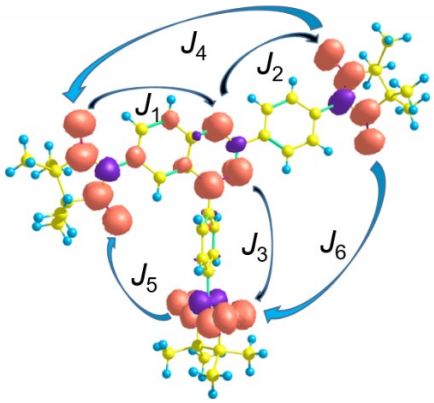

Figure 6. Spin density isosurface ($|\rho|$ = 0.0078 a. u.) calculated at the UB3LYP/def2-TZVP level for the quintet state and graphical representation of intramolecular exchange interactions for the Blt-$(NN)_3$ tetraradical.

Table 3. Parameters of intramolecular exchange interactions (numbering corresponds to Figure 6), calculated at different levels of theory using model diradicals (Figure S3.3, SI).

J_i, cm^{-1}	BS-DFT	CASSCF(10,10)	CASSCF(10,10)/ NEVPT2	Best-fitting parameters

J_1	562.3	251.9	247.8	245 ± 8
J_2	–65.9	–24.1	–17.1	–14.4 ± 0.5
J_3	46.3	7.5	9.3	3.9 ± 1.1
J_4	–22.6	–1.0	–1.4	–
J_5	–0.56	–0.1	–0.4	–
J_6	0.04	0.0	–0.4	–

Using the most accurate J values, calculated at CASPT2 level (Table 3), we evaluated the energies of the low-lying multiplets (Table 2). It is seen that these calculations also lead to the ground triplet state of the tetraradical, and neglecting $J_4 - J_6$ does not have a noticeable impact on the energies. Moreover, the complete splitting of the multiplets under consideration is similar for the two types of calculations, however, the latter calculations lead to a permutation of the lowest quintet and singlet states.

The temperature dependence of magnetic susceptibility is determined not only by intramolecular, but also by intermolecular exchange interactions, especially at cryogenic temperatures. Thus, we estimated also parameters of intermolecular interactions (J_i') using the BS-DFT approach, which works well in such cases.[3] Model radical pairs were used in these calculations (Figure S3.4 and discussion in Section S3, SI). Most of the J' parameters are very low (<1 cm^{-1} in absolute value), but two of them (–15.5 and 6.9 cm^{-1}) are predicted to be comparable in absolute magnitude to J_2 and J_3. Nevertheless, we had to use the mean-field approximation with parameter zJ' to account for intermolecular exchange interactions.

Thus, the temperature dependence of the magnetic susceptibility in the form of the χT vs T dependence (Figure 5) was approximated using the PHI software and the parameters J_1, J_2, and J_3 of the intramolecular exchange interaction and the mean-field parameter zJ'. The g-factor values were fixed and varied around g = 2.0. The best agreement with experiment was achieved for the following parameters: J_1 = 245 ± 8, J_2 = -14.4 ± 0.5, J_3 = 3.9 ± 1.1 cm^{-1} and zJ' = –0.76 ± 0.03 cm^{-1} at g = 1.98. The best-fitting parameters J_1 and J_2 are in perfect agreement with the calculations, while the best-fitting parameter J_3 has the same sign, but much greater uncertainty and about half the magnitude predicted by calculations (Table 3). Note that the negative value of zJ' is also consistent with the predicted predominance of antiferromagnetic intermolecular interactions.

We also recalculated the energies of the multiplets using the above $J_1 - J_3$ best-fit parameters and PHI software (Table 2). It can be seen that these calculations also lead to a ground triplet state with the same complete splitting as in previous calculations, but the splitting between the four lower multiplets is noticeably smaller than the previous one.

Electrochemistry and UV−Vis−Near-Infrared (NIR) Spectroscopy. Electrochemical parameters of the processes of oxidation and reduction of Blt-$(NN)_3$ tetraradical were determined by cyclic voltammetry (CV) on a glassy carbon disk electrode in a solution of an acetonitrile-based background electrolyte. On the oxidation curve for this compound, there is a peak at a potential of 0.45 V (I) and a cluster of two close peaks (II–III) in the potential range 0.70–1.20 V. On the reduction curve, there are three peaks at potentials –0.54 (IV), –1.10 (V), and –2.61 V (VI) (Figure 7).

For oxidation I peak and reduction IV peak, which have response peaks, a series of CV curves were recorded and analyzed at potential scan rates in the range of 0.05–1.00 V/s (Figures 8 and 9). According to the results, peak I matches chemically reversible oxidation of Blt-$(NN)_3$ tetraradical. It was found that the ratio of the reverse and forward peaks does not depend on the potential sweep rate and is close to 1.0 (I_p^{red}/I_p^{ox} = 0.98). The half-wave potential determined for this process is 0.41 V. The reduction of Blt-$(NN)_3$ tetraradical (peak IV) is chemically reversible too: the ratio of the reverse and forward peaks does not depend on the potential sweep rate and is 0.79. The noticeable difference between this value and 1.0 is due to a difficulty with determining the correct value of the background current for the response peak. Half-wave potential for this process is –0.51 V.

The oxidation II-III peaks and reduction V peak also have response waves (Figure 7). Nevertheless, in the case of peaks II-III, the degree of reversibility could not be determined due to a difficulty with determining the currents in each peak owing to an overlap with the signal of the "neighboring" process. For peak V, both the forward wave and backward wave have a complex shape, which is probably due to the course of at least two processes at close potentials, which cannot be separated either. The VI reduction peak is chemically irreversible (Figure 7).

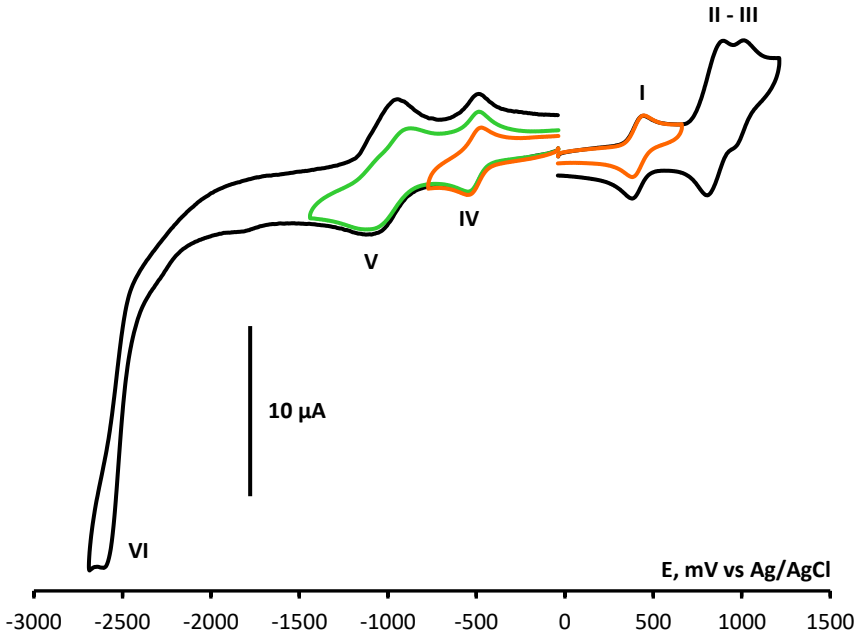

Figure 7. Cyclic voltammograms for Blt-$(NN)_3$ tetraradical (0.3×10^{-3} M) in 0.1 M Bu_4NBF_4/MeCN on a glassy carbon disk electrode at a potential sweep rate of 0.1 V/s. The orange and green curves show reversible/quasi-reversible behavior of peaks I, IV, and V.

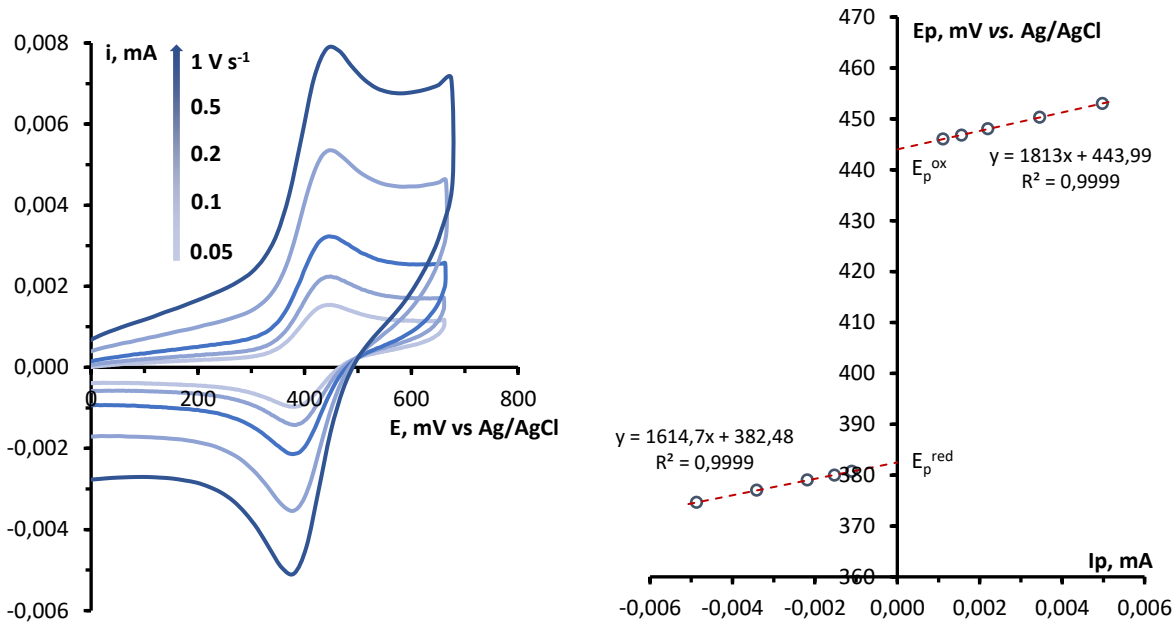

Figure 8. (left) CV curves for oxidation process I at potential scan rates of 0.05, 0.1, 0.2, 0.5, and 1.0 V/s. (right) Dependences of potentials of oxidation peaks and response reduction peaks on the current.

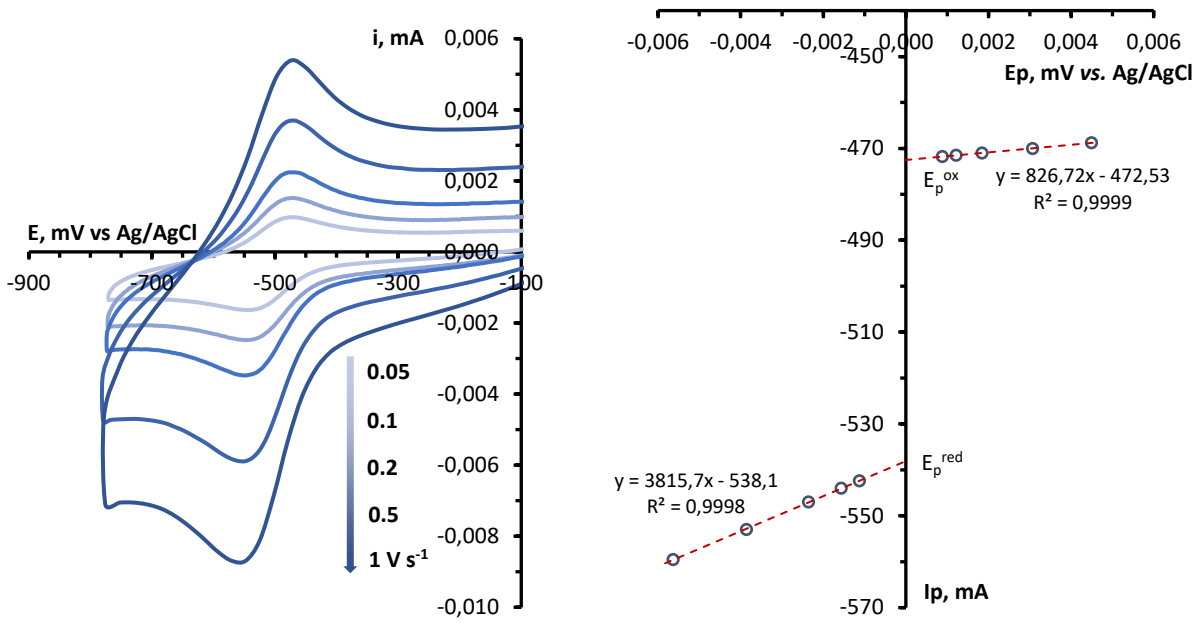

Figure 9. (left) CV curves for reduction process IV at potential scan rates of 0.05, 0.1, 0.2, 0.5, and 1.0 V/s. (right) Dependences of potentials of reduction peaks and response oxidation peaks on the current.

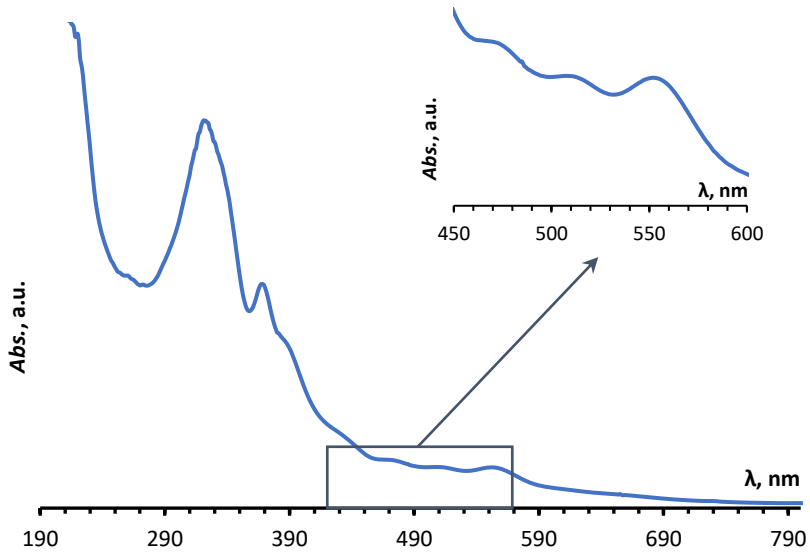

Figure 10. UV–Vis spectra of Blt-$(NN)_3$ tetraradical in MeCN, λ_{max}/nm (ε_{max}/L mol^{-1} cm^{-1}): 322 (9.32 × 10^3), 368 (5.39 × 10^3), 386 (4.04 × 10^3), 472 (1.16 × 10^3), 509 (0.99 × 10^3), and 552 (0.98 × 10^3). For phenyl-substituted nitronyl nitroxide in ethanol, the following spectral data have been reported, λ_{max}/nm (ε_{max}/L mol^{-1} cm^{-1}): 238 (9400), 263 (12200), 360 (13300), and 588 (685).[47] For triradical Blt-$(NN)_2$ in dichloromethane, the following spectra data have been reported, λ_{max}/nm (ε_{max}/L mol^{-1} cm^{-1}): 303 (3.49 × 10^4), 371 (2.26 × 10^4), 510 (5.26 × 10^3), and 545 (5.24 × 10^3).[35]

Thermal Stability. The Blt-$(NN)_3$ tetraradical possesses excellent stability under ambient conditions. It can be purified by chromatography on a normal-phase silica gel and stored under ambient conditions. Notably, solid Blt-$(NN)_3$ shows no signs of decomposition after storage in ambient air at −15 °C for more than 1 year. Our thermogravimetric analysis data suggested that after the loss of solvate molecules (7% mass loss), the thermal decomposition of Blt-$(NN)_3$ starts at ~150 °C (Figures S5.1 and S5.2), which is slightly lower than the onset temperature for triradical Blt-$(NN)_2$ (166 °C)[35] and that for diradical Blt-NN (160 °C).[34] The maximum rate of mass loss for Blt-$(NN)_3$ was registered at ~200 °C.

CONCLUSION

This paper reports the development of an efficient catalytic system for the cross-coupling of the tri-iodo-Blatter radical with a gold(I)−nitronyl nitroxide complex. We believe that this method will pave the way to the production of a variety of high-spin molecules. The proposed methodology made it possible to obtain the Blt-$(NN)_3$ tetraradical with a high-spin triplet ground state. Our tetraradical has three channels of efficient intramolecular exchange interaction: one channel with strong ferromagnetic interaction, the other two with moderate interactions of both types – ferro- and antiferromagnetic. The Blt-$(NN)_3$ tetraradical is stable in air and possesses high thermal stability in an inert atmosphere. It exhibits reversible redox waves (at −0.54 and 0.45 V vs Fc/Fc^+) unprecedented for high-spin tetraradicals. Magnetic properties of new tetraradical were characterized by SQUID magnetometry of polycrystalline powders and EPR spectroscopy in various matrices and analyzed with reference to X-ray diffraction (XRD) data and high-level quantum chemical calculations. The findings indicate that the Blt-$(NN)_3$ tetraradical has a triplet ground state and a nearby excited quintet state. Our tetraradical, due to its unprecedented combination of the high-spin ground state, thermal and electrochemical properties, can stimulate further development of purely organic magnetic and electronic materials.

EXPERIMENTAL SECTION

Reagents and General Methods

(Nitronyl nitroxide-2-ide)(triphenylphosphine)gold (NN-Au-PPh_3),[48] $Pd_2(dba)_3{\cdot}CHCl_3$,[49] and 1,3,5,7-tetramethyl-6-phenyl-2,4,8-trioxa-6-phosphaadamantane (^{Me}CgPPh)[50] were prepared according to procedures in the literature just cited. All other reagents were purchased from commercial suppliers and were used as received. Toluene was distilled under an argon stream and kept in an argon atmosphere. Other solvents were of reagent quality and used without additional purification. Reactions were monitored by thin-layer chromatography (TLC) on silica gel 60 F_{254} aluminum sheets from Merck. The chromatography was carried out on silica gel (0.050–0.160

mm) for column chromatography. Yields are given for pure substances obtained after recrystallization.

IR spectra were recorded with a Bruker Tensor 27 FTIR spectrometer in a KBr pellet. UV–Vis spectra were acquired in a MeCN solution on a Bruker Vector-22 spectrometer. CV measurements were performed in a glove box with an argon atmosphere and humidity and oxygen levels not exceeding 0.1 ppm using a standard three-electrode glass cell at potential scan rates of 0.05–1.00 $V \cdot s^{-1}$; the working electrode was a glassy carbon disk electrode with a disk diameter of 1.7 mm; the auxiliary electrode was a Pt wire calcined in the flame of a gas burner; the reference electrode was an Ag wire coated with a layer of AgCl; the reference electrode was calibrated relative to the ferrocene/ferrocenium pair (E^0 = 0.640 V rel. SHE); the background electrolyte was a 0.1 M solution of Bu_4NBF_4 in acetonitrile with a water content not exceeding 20 ppm.

All EPR data were collected using X/Q-band pulsed/CW EPR spectrometer Bruker Elexsys E580 equipped with an Oxford Instruments temperature control system. CW EPR spectra were obtained under conditions preventing modulation broadening and microwave saturation. FID-detected EPR spectra were obtained by integration of FID after a 1 μs microwave pulse. For all spectral simulations, the EasySpin toolbox for Matlab was utilized.[51]

Thermal analysis was performed on a TG/DTA Simultaneous Measuring Instrument, DTG-60 (Shimadzu). Experiment was carried out under argon flow at a heating rate of 10 °C/min in 25–500 ºC temperature interval.

Magnetic susceptibility of polycrystalline samples was measured with a Quantum Design MPMS*XL* SQUID magnetometer in the temperature range 2–300 K in a magnetic field of up to 5 kOe. Diamagnetic corrections were made using Pascal constants.[52] The spin Hamiltonian in the general form of $H = -2J\hat{\vec{S}}_1\hat{\vec{S}}_2$ was employed for an analysis of the experimental $\chi(T)T$ dependencies.

Synthesis of Triradical Blt-(NN)$_3$. A 10-mL vial purged with argon was charged with a magnetic stir bar, Blt-I_3 (0.050 g, 0.076 mmol, 1.0 equiv.), NN-Au-PPh_3 (0.164 g, 0.266 mmol, 3.5 equiv.), $Pd_2(dba)_3 \cdot CHCl_3$ (0.031 g, 0.030 mmol, 0.4 equiv.), and ^{Me}CgPPh (0.035 g, 0.122 mmol, 1.6 equiv.). Then, toluene (5 mL) was added into the vial. After stirring for 20 h at room temperature (~19 °C), the reaction mixture almost did not contain the initial NN-Au-PPh_3 (as evidenced by TLC). Then, the reaction solution (in toluene) was loaded onto a silica gel column wetted with hexane. Elution with $CHCl_3$, followed by hexane-EtOAc (1:1), followed by EtOAc gave the target tetraradical Blt-(NN)$_3$ as a dark brown solid. Yield: 0.047 g (82%). TLC R_f = 0.50 (EtOAc). Crystals suitable for XRD were obtained by slow evaporation of a CH_2Cl_2/heptane solution at 5 °C for 1 day in an open vial. IR (KBr, cm^{-1}): 3486, 3056, 2987, 2933, 2870, 2586,

1734, 1636, 1596, 1517, 1482, 1451, 1436, 1422, 1390, 1364, 1309, 1273, 1217, 1182, 1166, 1134, 1071, 1018, 994, 921, 867, 843, 756, 722, 695, 638, 618, 595, 542, 453, 413. High-resolution mass spectrometry (m/z): calcd for $C_{40}H_{47}N_9O_6$ $[M]^+$: 749.3649. Found: 749.3637.

X-ray Crystallography. Intensity data from a single crystal of Blt-$(NN)_3$ were collected on a Bruker AXS diffractometer: Apex Duo (Cu Kα, λ = 1.54178 Å, room temperature). Absorption correction was applied by means of Bruker SADABS (version 2.10).[53] The structure was solved by direct methods and refined by the full-matrix least-squares method in an anisotropic approximation for all nonhydrogen atoms. Positions of the H atoms were computed geometrically and included in the refinement in a riding model. All calculations for structure solution and refinement were performed in the SHELXL-2018/3 software.[54,55] Crystallographic data were deposited with the Cambridge Crystallographic Data Centre and can be obtained free of charge via http://www.ccdc.cam.ac.uk/conts/retrieving.html (or from the CCDC, 12 Union Road, Cambridge CB2 1EZ, UK; Fax: +44 1223 336033; E-mail: deposit@ccdc.cam.ac.uk).

Crystallographic data for Blt-$(NN)_3$: $C_{41}H_{49}Cl_2N_9O_6$, M = 834.79, T = 296 K, monoclinic space group $P2_1/c$, a = 25.273(6), b = 12.106(3), c = 13.814(4) Å, β = 93.554(16)°, V = 4218.6(18) Å^3; Z = 4, ρ_{calc} = 1.314 g·cm^{-3}, μ(Cu Kα) = 1.856 mm^{-1}, θ range 3.504–68.309°, I_{hkl} collected/unique 52041/7667, R_{int} = 0.1627, 3654 I_{hkl} with $I > 2\sigma(I)$, 524 refined parameters, *GooF* = 0.933, R_1 = 0.0747, wR_2 = 0.2044, CCDC 2252621.

Computational Details. The spin density distribution for the Blt-$(NN)_3$ tetraradical in the high-spin quintet state was calculated at the UB3LYP/def2-TZVP level.[56–57,58] The energies of the lowest energy multiplets, arising from the exchange interactions of the radical fragments, were calculated at the CASSCF[59] and CASSCF/NEVPT2[60] levels of theory using XRD geometry with the def2-TZVP basis set. The parameters J_{ij} of exchange interactions between radical fragments ($\hat{H}_{ij} = -2J_{ij}\hat{\hat{S}}_i\hat{\hat{S}}_j$) were calculated for the model diradicals, which were obtained from a tetraradical structure by adding two hydrogen atoms to the rest two radical centers. These parameters were calculated at the CASSCF and NEVPT2 levels, as well as using the spin-unrestricted broken-symmetry (BS) approach[61] at the BS-B3LYP/def2-TZVP level of theory using the Yamaguchi formula[62] $J = -\frac{E^{HS}-E_{BS}^{LS}}{\langle S^2\rangle^{HS}-\langle S^2\rangle_{BS}^{LS}}$. Using the PHI program[63] and the calculated parameters, the energies of the lower states of Blt-$(NN)_3$ were also recalculated.

ASSOCIATED CONTENT

Supporting Information

The Supporting Information is available free of charge at https://pubs.acs.org/doi/.

Bulk crystal sample, additional EPR data, computation details, FT-IR and UV-vis spectra, and thermogravimetric analysis (PDF)

Accession Codes

CCDC 2252621 contains the supplementary crystallographic data for this paper. These data can be obtained free of charge via www.ccdc.cam.ac.uk/data_request/cif, or by emailing data_request@ccdc.cam.ac.uk, or by contacting the Cambridge Crystallographic Data Centre, 12 Union Road, Cambridge CB2 1EZ, UK; fax: +44 1223 336033.

ACKNOWLEDGMENTS

G.V.R. and A.S.B. thank the Russian Science Foundation (grant 23-13-00014) for supporting of a part of this research (single-crystal XRD and magnetochemistry), A.A.D. and N.P.G. acknowledge the core funding from the Russian Federal Ministry of Science and Higher Education (project FWGF-2021-0002) for support of the computational part of this paper and the Research Resource Center “Irkutsk Supercomputer Center SB RAS” for the computational resources.

REFERENCES

(1) Rajca, A.; Mukherjee, S.; Pink, M.; Rajca, S. Exchange Coupling Mediated Through-Bonds and Through-Space in Conformationally Constrained Polyradical Scaffolds: Calix[4]arene Nitroxide Tetraradicals and Diradical. *J. Am. Chem. Soc*. **2006**, *128*, 13497−13507.

(2) Burnea, F. K. B.; Nam, Y.; Lee, J. Y. H-Bonding on spin centres enhances spin−spin coupling for organic diradicals. *J. Mater. Chem. C* **2020**, *8*, 3402−3408.

(3) Tretyakov, E. V.; Zhivetyeva, S. I.; Petunin, P. V.; Gorbunov, D. E.; Gritsan, N. P.; Bagryanskaya, I. Y.; Bogomyakov, A. S.; Postnikov, P. S.; Kazantsev, M. S.; Trusova, M. E.; Shundrina, I. K.; Zaytseva, E. V.; Parkhomenko, D. A.; Bagryanskaya, E. G.; Ovcharenko, V. I. Ferromagnetically Coupled *S*=1 Chains in Crystals of Verdazyl-Nitronyl Nitroxide Diradicals. *Angew. Chem*. *Int. Ed.* **2020**, *59* (46), 20704–20710.

(4) Tretyakov, E. V.; Petunin, P. V.; Zhivetyeva, S. I.; Gorbunov, D. E.; Gritsan, N. P.; Fedin, M. V.; Stass, D. V.; Samoilova, R. I.; Bagryanskaya, I. Y.; Shundrina, I. K.; Bogomyakov, A. S.; Kazantsev, M. S.; Postnikov, P. S.; Trusova, M. E.; Ovcharenko, V. I. Platform for High-Spin Molecules: A Verdazyl-Nitronyl Nitroxide Triradical with Quartet Ground State. *J. Am. Chem. Soc.* **2021**, *143* (21), 8164−8176.

(5) Chen, Z. X.; Li, Y.; Huang, F. Persistent and Stable Organic Radicals: Design, Synthesis, and Applications. *Chem* **2021**, *7* (2), 288–332.

(6) Nishide, H.; Oyaizu, K. Toward Flexible Batteries. *Science* **2008**, *319*, 737−738.

(7) Morita, Y.; Nishida, S.; Murata, T.; Moriguchi, M.; Ueda, A.; Satoh, M.; Arifuku, K.; Sato, K.; Takui, T. Organic tailored batteries materials using stable open-shell molecules with degenerate frontier orbitals. *Nat. Mater*. **2011**, *10*, 947−951.

(8) Ratera, I.; Veciana, J. Playing with organic radicals as building blocks for functional molecular materials. *Chem. Soc. Rev*. **2012**, *41*, 303−349.

(9) Gallagher, N. M.; Olankitwanit, A.; Rajca, A. High-Spin Organic Molecules. *J. Org. Chem*. **2015**, *80*, 1291−1298.

(10) Rocha, A. R.; García-Suárez, V. M.; Bailey, S. W.; Lambert, C. J.; Ferrer, J.; Sanvito, S. Towards molecular spintronics. *Nat. Mater*. **2005**, *4*, 335−339.

(11) Mas-Torrent, M.; Crivillers, N.; Mugnaini, V.; Ratera, I.; Rovira, C.; Veciana, J. Organic radicals on surfaces: towards molecular spintronics. *J. Mater. Chem*. **2009**, *19*, 1691−1695.

(12) Sanvito, S. Molecular spintronics. *Chem. Soc. Rev*. **2011**, *40*, 3336−3355.

(13) Herrmann, C.; Solomon, G. C.; Ratner, M. A. Organic Radicals as Spin Filters. *J. Am. Chem. Soc*. **2010**, *132*, 3682−3684.

(14) Bajaj, A.; Khurana, R.; Ali, M. E. Quantum interference and spin filtering effects in photo-responsive single molecule devices. *J. Mater. Chem. C* **2021**, *9*, 11242−11251.

(15) Shil, S.; Bhattacharya, D.; Misra, A.; Klein, D. J. A high-spin organic diradical as a spin filter. *Phys. Chem. Chem. Phys*. **2015**, *17*, 23378−23383.

(16) Zhang, B.; Chen, Y.; Neoh, K-G.; Kang, E-T. Organic Electronic Memory Devices. In *Electrical Memory Materials and Devices*; Chen, W. C., Ed.; The Royal Society of Chemistry: Cambridge, UK, 2015, Vol. 4, 1−53. DOI: 10.1039/9781782622505-00001

(17) Gaudenzi, R.; De Bruijckere, J.; Reta, D.; Moreira, I. D. P.; Rovira, C.; Veciana, J.; Van Der Zant, H. S.; Burzurí, E. Redox-Induced Gating of the Exchange Interactions in a Single Organic Diradical. *ACS Nano* **2017**, *11*, 5879−5883.

(18) Tsuji, Y.; Hoffmann, R.; Strange, M.; Solomon, G. C. Close relation between quantum interference in molecular conductance and diradical existence. *Proc. Natl. Acad. Sci. U.S.A*. **2016**, *113*, E413–E419

(19) Gaudenzi, R.; Burzuri, E.; Reta, D.; Moreira, I. de P. R.; Bromley, S. T.; Rovira, C.; Veciana, J.; van der Zant, H. S. J. Exchange Coupling Inversion in a High-Spin Organic Triradical Molecule. *Nano Lett*. **2016**, *16*, 2066−2071.

(20) Khurana, R.; Bajaj, A.; Shamasundar, K. R.; Ali, Md. E. High-Spin Blatter's Triradicals. *J. Phys. Chem. A* **2023**, *127* (37), 7802–7810.

(21) *Stable Radicals: Fundamentals and Applied Aspects of Odd-Electron Compounds*; Hicks, R. G., Ed.; John Wiley & Sons, Ltd.: Chichester, UK, 2010. DOI:10.1002/9780470666975

(22) Blatter, H. M.; Lukaszewski, H. A new stable free radical. *Tetrahedron Lett*. **1968**, *9*, 2701−2705.

(23) Koutentis, P. A.; Lo Re, D. Catalytic Oxidation of *N*-Phenylamidrazones to 1,3-Diphenyl-1,4-dihydro-1,2,4-benzotriazin-4-yls: An Improved Synthesis of Blatter′s Radical. *Synthesis* **2010**, 2075−2079.

(24) Constantinides, C. P.; Obijalska, E.; Kaszyński, P. Access to 1,4-Dihydrobenzo[*e*][1,2,4]triazin-4-yl Derivatives. *Org. Lett*. **2016**, *18* (5), 916−919.

(25) Kaszyński, P.; Constantinides, C. P.; Young Jr., V. G., The Planar Blatter Radical: Structural Chemistry of 1,4-Dihydrobenzo[*e*][1,2,4]triazin-4-yls. *Angew. Chem*. **2016**, *128*, 11315−11318.

(26) Bartos, P.; Hande, A. A.; Pietrzak, A.; Chrostowska, A.; Kaszyński, P. Substituent effects on the electronic structure of the flat Blatter radical: correlation analysis of experimental and computational data. *New J. Chem*. **2021**, *45*, 22876−22887.

(27) Gulyaev, D.; Serykh, A.; Tretyakov, E.; Akyeva, A.; Syroeshkin, M.; Gorbunov, D. E.; Maltseva, S. V.; Gritsan, N. P.; Romanenko, G.; Bogomyakov, A. Effects of Difluorophenyl Substituents on Structural, Redox, and Magnetic Properties of Blatter Radicals. *Catalysts* **2023**, *13*, 1206.

(28) Rogers, F. J.; Norcott, P. L.; Coote, M. L. Recent advances in the chemistry of benzo[*e*][1,2,4]triazinyl radicals. *Org. Biomol. Chem.* **2020**, *18*, 8255–8277.

(29) Ji, Y.; Long, L.; Zheng, Y. Recent advances of stable Blatter radicals: synthesis, properties and applications. *Mater. Chem. Front*. **2020**, *4*, 3433–3443.

(30) Baumgarten, M. High Spin Organic Molecules. In *World Scientific Reference on Spin in Organics*; Miller, J. S.; Vardeny Z. V.; Wohlgenannt M., Eds.; World Scientific Publishing Co. Pte. Ltd.: Singapore, 2018, Vol. 4, 1–93. DOI: 10.1142/9789813230200_0001

(31) Ovcharenko, V. I.; Terent′ev, A. O.; Tretyakov, E. V.; Krylov, I. B. From the chemistry of radicals to molecular spin devices. *Russ. Chem. Rev*. **2022**, *91*, RCR5043.

(32) Rajca, A. Magnetism of Nitroxides. In *Nitroxides: Synthesis, Properties and Applications*. Ouari, O.; Gigmes, D., Eds.; The Royal Society of Chemistry: Cambridge: London, UK, 2021, 359–391. DOI: 10.1039/9781788019651-00359

(33) Gallagher, N. M.; Bauer, J. J.; Pink, M.; Rajca, S.; Rajca, A. High-Spin Organic Diradical with Robust Stability. *J. Am. Chem. Soc*. **2016**, *138*, 9377−9380.

(34) Gallagher, N.; Zhang, H.; Junghoefer, T.; Giangrisostomi, E.; Ovsyannikov, R.; Pink, M.; Rajca, S.; Casu, M. B.; Rajca, A. Thermally and Magnetically Robust Triplet Ground State Diradical. *J. Am. Chem. Soc*. **2019**, *141*, 4764−4774.

(35) Shu, C.; Pink, M.; Junghoefer, T.; Nadler, E.; Rajca, S.; Casu, M. B.; Rajca, A. Synthesis and Thin Films of Thermally Robust Quartet (S = 3/2) Ground State Triradical. *J. Am. Chem. Soc*. **2021**, *143*, 5508−5518.

(36) Rajca, A.; Utamapanya, S. Poly(arylmethyl) Quartet Triradicals and Quintet Tetraradicals. *J. Am. Chem. Soc*. **1993**, *115*, 2396–2401.

(37) Rajca, A.; Olankitwanit, A.; Wang, Y.; Boratyński, P. J.; Pink, M.; Rajca, S. High-Spin S = 2 Ground State Aminyl Tetraradicals. *J. Am. Chem. Soc*. **2013**, *135*, 18205−18215.

(38) Rajca, A.; Boratyński, P. J.; Olankitwanit, A.; Shiraishi, K.; Pink, M.; Rajca, S. Ladder Oligo(*m*-aniline)s: Derivatives of Azaacenes with Cross-Conjugated π-Systems. *J. Org. Chem*. **2012**, *77* (5), 2107−2120.

(39) Tanimoto, R.; Suzuki, S.; Kozaki, M.; Okada, K. Nitronyl Nitroxide as a Coupling Partner: Pd-Mediated Cross-coupling of (Nitronyl nitroxide-2-ido)(triphenylphosphine)gold(I) with Aryl Halides. *Chem. Lett*. **2014**, *43*, 678−680.

(40) Tahara, T.; Suzuki, S.; Kozaki, M.; Shiomi, D.; Sugisaki, K.; Sato, K.; Takui, T.; Miyake, Y.; Hosokoshi, Y.; Nojiri, H.; Okada, K. Triplet Diradical-Cation Salts Consisting of the Phenothiazine Radical Cation and a Nitronyl Nitroxide. *Chem. Eur. J*. **2019**, *25*, 7201−7209.

(41) Tretyakov, E. V.; Ovcharenko, V. I.; Terent′ev, A. O.; Krylov, I. B.; Magdesieva, T. V.; Mazhukin, D. G.; Gritsan, N. P. Conjugated nitroxides. *Russ. Chem. Rev*. **2022**, *91* (2), RCR5025.

(42) Zayakin, I.; Bagryanskaya, I.; Stass, D.; Kazantsev, M.; Tretyakov, E. Synthesis and Structure of (Nitronyl Nitroxide-2-ido)(tert-butyldiphenylphosphine)gold(I) and -(Di(tert-butyl)phenylphosphine)gold(I) Derivatives; Their Comparative Study in the Cross-Coupling Reaction. *Crystals* **2020**, *10* (9), 770.

(43) Zayakin, I. A.; Korlyukov, A. A.; Gorbunov, D. E.; Gritsan, N. P.; Akyeva, A. Ya.; Syroeshkin, M. A.; Stass, D. V.; Tretyakov, E. V.; Egorov, M. P. Au–Au Chemical Bonding in Nitronyl Nitroxide Gold(I) Derivatives. *Organometallics* **2022**, *41*, 1710.

(44) Zayakin, I.; Tretyakov, E.; Akyeva, A.; Syroeshkin, M.; Burykina, Ju.; Dmitrenok, A.; Korlyukov, A.; Nasyrova, D.; Bagryanskaya, I.; Stass, D.; Ananikov, V. Overclocking Nitronyl Nitroxide Gold Derivatives in Cross-Coupling Reactions. *Chem. Eur. J*. **2022**, e202203118.

(45) Bencini, A.; Gatteschi D. Electron Paramagnetic Resonance of Exchange Coupled Systems. Springer-Verlag: Berlin, Heidelberg, 1990, pp. 287. DOI: 10.1007/978-3-642-74599-7

(46) McConnell, H. M. Ferromagnetism in Solid Free Radicals. *J. Chem. Phys.* **1963**, *39*, 1910.

(47) Osiecki, J. H.; Ullman, E. F. Studies of Free Radicals. I. α-Nitronyl Nitroxides, a New Class of Stable Radicals. *J. Am. Chem. Soc*. **1968**, *90*, 1078–1079.

(48) Suzuki, S.; Kira, S.; Kozaki, M.; Yamamura, M.; Hasegawa, T.; Nabeshima, T.; Okada, K. An efficient synthetic method for organometallic radicals: structures and properties of gold(I)-(nitronyl nitroxide)-2-ide complexes. *Dalton Trans.* **2017**, *46* (8), 2653–2659.

(49) Zalesskiy, S. S., Ananikov, V. P. $Pd_2(dba)_3$ as a Precursor of Soluble Metal Complexes and Nanoparticles: Determination of Palladium Active Species for Catalysis and Synthesis. *Organometallics* **2012**, *31* (6), 2302–2309.

(50) Le, C. M.; Hou, X.; Sperger, T.; Schoenebeck, F.; Lautens, M. An Exclusively *trans*-Selective Chlorocarbamoylation of Alkynes Enabled by a Palladium/Phosphaadamantane Catalyst. *Angew. Chem. Int. Ed*. **2015**, *54* (52), 15897–15900.

(51) Cai, S.; Chen, C.; Sun, Z.; Xi, C. CuCl-catalyzed orthotrifluoromethylation of arenes and heteroarenes with a pivalamido directing group. *Chem. Commun.* **2013**, *49* (40), 4552–4554.

(52) Carlin, R. L. Magnetochemistry. Springer-Verlag: Berlin, Heidelberg, 1986. DOI: 10.1007/978-3-642-70733-9

(53) Krause, L.; Herbst-Irmer, R.; Sheldrick, G. M.; Stalke, D. Comparison of silver and molybdenum microfocus X-ray sources for single-crystal structure determination. *J. Appl. Crystallogr.* **2015**, *48*, 3–10.

(54) Sheldrick, G. M. SHELXT – Integrated space-group and crystal-structure determination. *Acta Crystallogr. Sect. A Found. Crystallogr.* **2015**, *71* (1), 3–8.

(55) Sheldrick, G. M. Crystal structure refinement with *SHELXL*. *Acta Crystallogr. C Struct. Chem*. **2015**, *71*, 3–8.

(56) Lee, C.; Yang, W.; Parr, R. G. Development of the Colle-Salvetti correlation-energy formula into a functional of the electron density. *Phys. Rev. B* **1988**, *37* (2), 785–789.

(57) Becke, A. D. Density-functional thermochemistry. III. The role of exact exchange. *J. Chem. Phys.* **1993**, *98* (7), 5648–5652.

(58) Weigend, F.; Ahlrichs, R. Balanced Basis Sets of Split Valence, Triple Zeta Valence and Quadruple Zeta Valence Quality for H to Rn: Design and Assessment of Accuracy. *Phys. Chem. Chem. Phys.* **2005**, *7* (18), 3297–3305.

(59) Frisch, M.; Ragazos, I. N.; Robb, M. A.; Bernhard Schlegel, H. An evaluation of three direct MC-SCF procedures. *Chem. Phys. Lett.* **1992**, *189* (6), 524–528.

(60) Angeli, C.; Cimiraglia, R.; Evangelisti, S.; Leininger, T.; Malrieu, J. P. Introduction of *n*-electron valence states for multireference perturbation theory. *J. Chem. Phys.* **2001**, *114* (23), 10252.

(61) Nagao, H.; Nishino, M.; Shigeta, Y.; Soda, T.; Kitagawa, Y.; Onishi, T.; Yoshioka, Y.; Yamaguchi, K. Theoretical studies on effective spin interactions, spin alignments and

macroscopic spin tunneling in polynuclear manganese and related complexes and their mesoscopic clusters. *Coord. Chem. Rev.* **2000**, *198* (1), 265–295.

(62) Soda, T.; Kitagawa, Y.; Onishi, T.; Takano, Y.; Shigeta, Y.; Nagao, H.; Yoshioka, Y.; Yamaguchi, K. Ab initio computations of effective exchange integrals for H–H, H–He–H and Mn_2O_2 complex: comparison of broken-symmetry approaches. *Chem. Phys. Lett.* **2000**, *319* (3–4), 223–230.

(63) Chilton, N. F.; Anderson, R. P.; Turner, L. D.; Soncini, A.; Murray, K. S. PHI: A powerful new program for the analysis of anisotropic monomeric and exchange-coupled polynuclear *d*- and *f*-block complexes. *J. Comput. Chem.* **2013**, *34*, 1164–1175.